JGR Planets

RESEARCH ARTICLE

10.1029/2024JE008550

Initial Thermal States of Super-Earth Exoplanets and Implications for Early Dynamos

Nathaniel I. White[1] and **Jie Li**[1]

[1]Department of Earth and Environmental Sciences, University of Michigan, Ann Arbor, MI, USA

Key Points:

- Gravitational energy associated with core formation increases with planet mass for super-Earths with Earth-like composition
- Accretion and differentiation in most super-Earth exoplanets generate enough heat to at least partially melt their cores, thus allowing the formation of early magnetic fields
- The largely molten state of Earth's core suggests that at least 7% accretional energy contributed to the initial heating of rocky planets

Supporting Information:

Supporting Information may be found in the online version of this article.

Correspondence to:

J. Li,
jackieli@umich.edu

Citation:

White, N. I., & Li, J. (2025). Initial thermal states of super-Earth exoplanets and implications for early dynamos. *Journal of Geophysical Research: Planets*, *130*, e2024JE008550. https://doi.org/10.1029/2024JE008550

Received 4 JUN 2024
Accepted 2 FEB 2025

Author Contributions:

Conceptualization: Nathaniel I. White, Jie Li
Data curation: Nathaniel I. White
Formal analysis: Nathaniel I. White
Investigation: Nathaniel I. White
Methodology: Nathaniel I. White, Jie Li
Project administration: Jie Li
Resources: Jie Li
Software: Nathaniel I. White
Supervision: Jie Li
Validation: Nathaniel I. White, Jie Li
Visualization: Nathaniel I. White
Writing – original draft: Nathaniel I. White, Jie Li
Writing – review & editing: Nathaniel I. White, Jie Li

Abstract The accretion of Earth and the formation of a metallic core released a large amount of primordial heat and may have enabled its evolution into a habitable world. Metal-silicate segregation likely occurs in super-Earth exoplanets as well, but its influence on their initial thermal states has not been fully examined. Here we calculated the energy released during core-mantle differentiation of super-Earths for a range of planet radii and core mass fractions. We found that the energy of differentiation increases with planet mass for rocky planets with Earth-like composition, and it peaks at 55% core by mass in Earth-sized rocky planets. Using the latest mineral physics constraints on the equations-of-state and melting curve of relevant phases, we modeled the initial thermal profiles and assessed the extent of melting in initial iron cores for plausible heat retention efficiencies. Our results suggest that following accretion and metal-silicate differentiation, the cores of most super-Earths are expected to be at least partially molten, a necessary condition for the generation of a magnetic field. Based on the largely molten state of Earth's core at the present day, we place a lower bound of 7% retention of accretional energy as primordial heat in rocky planets.

Plain Language Summary A protective magnetic field is widely considered a prerequisite for planetary habitability. Super-Earths are exoplanets with a rocky composition and up to twice the Earth's radius. Like Earth, these planets acquire a large amount of primordial heat during their birth and differentiation. This study aims to evaluate the potential of super-Earth exoplanets to develop early magnetic fields. We calculated the energies of accretion and metal-silicate segregation. This was done for a range of planet radii and core mass fractions. Furthermore, we modeled the internal pressures and initial thermal states of super-Earth planets, considering various heat retention efficiencies. We then compared the core temperature profiles with the melting curve of iron to determine the extent of melting in the core. Our results suggest that most super-Earth planets could acquire enough heat to at least partially melt their cores. This would allow the generation of global magnetic fields and therefore support habitability.

1. Introduction

To date, more than 5,000 exoplanets have been confirmed, about half of which were discovered in just the last 14 years by the Kepler Space Telescope (Abushattal et al., 2022). This increase in the number of known exoplanets also comes with improved accuracy and precision of available measurements, mainly external properties such as mass and radius. Super-Earths make up nearly one-third of the currently known exoplanets. They are defined as terrestrial planets with 1 and 2 Earth radii (R_E) and 1 to 10 Earth masses (M_E), as more massive planets are expected to acquire a significant gaseous envelope and become mini-Neptunes (Izidoro et al., 2022; Spiegel et al., 2013; Zeng et al., 2021). With a rocky surface potential to develop magnetic fields, super-Earths represent strong candidates for habitable worlds and are thus objects of great interest (Duffy et al., 2015; Hu et al., 2019).

The relationship between magnetic fields and planetary habitability is an area of ongoing research. A global magnetic field shields a planet's atmosphere from cosmic rays and stellar radiation; thus, it has been widely considered a necessary component of the habitability paradigm (Gunell et al., 2018; Kaltenegger, 2017). Although no exoplanet magnetic fields have been detected yet, such measurements could place constraints on the planet's internal structure and thermal state. The operation of a planetary dynamo requires rapid convection of a conductive fluid, which in a super-Earth is presumably molten iron in the core. In the Earth, inner core solidification is posited to have supplied much of the required dynamo power. However, the inner core may have only existed for the past 0.5 to 1.0 billion years, while the geomagnetic field is significantly longer-lived, leading to the "new core paradox" (Olson, 2013). Other than a liquid core, sustaining a magnetic field also requires favorable impact conditions, ohmic dissipation parameters, and convective motions (Monteux et al., 2011).

The potential of super-Earth exoplanets for developing dynamo depends on their thermal state. A recent study by Boujibar et al. (2020) calculated the thermal energy generated by accretion and suggested that larger super-Earths are likely to have an initial crystallizing core to help maintain a magnetic field. They built internal structure models and quantified various factors involved in planetary formation. As acknowledged, however, the study ignored differentiation and therefore underestimated the core temperature of a planet that has undergone metal-silicate segregation. As a result, the initial temperature at the Earth's core-mantle boundary (CMB) was estimated at 3,615 K, below the current temperature at CMB and the melting points of relevant iron-alloys at the CMB pressure (Li, 2021; Li et al., 2019). This is inconsistent with the geophysical observation that more than 90% of the Earth's core is molten at present (Dziewonski & Anderson, 1981), and that it was likely fully molten shortly after formation (Buffett et al., 1996). Therefore, it is necessary to consider the contribution of the energy of differentiation to the initial thermal states of super-Earth exoplanets.

The process of core-mantle differentiation refers to the separation of iron-rich metal from silicate in the early stages of planetary development (Cambioni et al., 2021). Depending on the planet size and relative size of the core, a large amount of potential energy may be released as heat when the planet evolves from the undifferentiated state consisting of a homogeneous mixture of iron alloy and silicate to the differentiated state with an iron core inside a silicate mantle. Here, we calculate the energies of accretion and differentiation of super-Earth exoplanets for a range of planetary radii, core mass fraction (CMF), and heat retention efficiencies. Then, we model the internal structure and initial thermal states of differentiated planets to determine the physical state of their iron cores. Our models incorporate recent results on material properties, including the latest equations of state (EoS) of Fe and $MgSiO_3$ at the pressure conditions of super-Earth exoplanets. Furthermore, by comparing the predicted and known thermal states of planetary bodies within the Solar System, we place constraints on the retention efficiencies of heat derived from accretion and differentiation.

2. Methods

2.1. Calculate Energy of Differentiation

The accretion of dispersed source material into a planet releases potential energy, part of which is converted to heat and retained by the planet as part of its primordial heat. The potential energy of accretion may be calculated for an undifferentiated rocky planet consisting of well-mixed iron and silicate, U_u. This corresponds to the reduction of gravitational energy with respect to dispersed ingredients. As the rocky planet undergoes differentiation to form an iron core enclosed in a silicate mantle, more gravitational energy is released to reach U_d, which corresponds to the reduction of gravitational energy with respect to dispersed building blocks.

For simplicity, we consider a two-component planet consisting of pure iron and pure $MgSiO_3$ silicate, with a total mass of M and a core mass fraction CMF. To calculate the total gravitational energy released during accretion and differentiation, we assume that iron and silicate are fully incompressible. A small fraction of these energies converts into elastic energy stored in a compressed planet and most of them convert to heat through friction (Birch, 1965; Flasar & Birch, 1973). The U_u and U_d are calculated by

$$U = \int_0^M \frac{Gm}{r(m)} dm \tag{1}$$

where G is the gravitational constant $6.6743 \cdot 10^{-11}$ N m^1 kg^{-2}, $r(m)$ is a function of radius with respect to mass. The energy of differentiation U_u–U_d corresponds to the further reduction of gravitational energy from the undifferentiated state to the differentiated state.

2.2. Structure Modeling

To estimate the internal properties of a differentiated rocky planet consisting of an iron (Fe) core inside a $MgSiO_3$ silicate mantle, we constructed a finite-element iterative algorithm, where a planet is divided into concentric spherical shells, each with a uniform density, pressure, and gravitational acceleration (Figure S1 in Supporting Information S1). Starting with the planet radius, core radius fraction (CRF), and an initial density ρ_0 at 1 bar and 300 K and assuming hydrostatic equilibrium, the algorithm calculates the gravity profile and then the pressure

profile in the first iteration. It then updates the density profile according to relevant equations of state (EoS), recalculates the gravity profile, and recalculates the pressure profile in the next iteration. Iterations are repeated until the density changes fall below 10 kg m^{-3}. At the end, the algorithm produces planet mass, core mass fraction (CMF), and a final pressure profile as the output.

We adopted the Rose-Vinet equation of state (EoS) parameters of $MgSiO_3$ by Fei et al. (2021), which showed excellent agreement between experimental data and theoretical predications. Parameters for the EoS of Fe were based on Smith et al. (2018), with significantly reduced uncertainties compared with previous studies. Crude approximations were made to account for thermal expansion and molten state of iron in the core: After applying the EoS at 300 K, we took a 12.5% reduction in final density to account for the volume of fusion for iron (~2%), the average thermal expansion between 300 and 5,000 K (~4%), and the presence of light elements (~6.5%) (Komabayashi & Fei, 2010; Li & Fei, 2014; Smith et al., 2018). In the mantle, thermal expansion and the presence of iron contributed −3% and +3% to density, respectively, effectively canceling each other out (Fei et al., 2021; Liu et al., 2018). We therefore applied the EoS at 300 K to calculate the density without further adjustments.

2.3. Model Initial Thermal State

The energy of accretion and differentiation would be partially converted into heat through friction and heat up the planet. Boujibar et al. (2020) estimated the temperatures of super-Earth exoplanets following accretion. We built on their work by adding a term for temperature rise due to the energy of differentiation:

$$T = T_i + \Delta T_G + \Delta T_D + \Delta T_{ad} \tag{2}$$

where T is the average temperature at the core-mantle boundary (CMB) of a planet after its formation and early differentiation, T_i is the initial temperature of radiative equilibrium at a planet's orbit, ΔT_G is the temperature rise due to accretion, and ΔT_D is the temperature rise due to differentiation, and ΔT_{ad} is the adiabatic gradient, which accounts for the increase in temperature with depth as a result of adiabatic compression.

The initial temperature of radiative equilibrium T_i is assumed to be 255 K, the value at Earth's orbit. The temperature rise due to accretion is calculated as

$$\Delta T_G = f_G \frac{U_U}{C} \tag{3}$$

Where U_u is the energy of accretion, f_G is the heat retention factor, that is, the fraction of energy of accretion that contributes to heating the planet, and C is the average specific heat capacity calculated as

$$C = C^{Fe}\,\mathrm{CMF} + C^{MgSiO_3}(1 - \mathrm{CMF}) \tag{4}$$

where the specific heat capacity of Fe and $MgSiO_3$, C^{Fe} and C^{MgSiO_3} are estimated using the Dulong-Petit law at 1,250 $J{\cdot}kg^{-1}{\cdot}K^{-1}$ and 450 $J{\cdot}kg^{-1}{\cdot}K^{-1}$, respectively (Poirier, 2000), and CMF is the core mass fraction.

The temperature rise due to differentiation is calculated as

$$\Delta T_D = \frac{f_D}{C}(U_U - U_D) \tag{5}$$

where $U_U - U_D$ is the energy of differentiation, f_D is the heat retention factor during differentiation and C is the average specific heat capacity.

The adiabatic temperature gradient is calculated as

$$\frac{dT}{dP} = \frac{\gamma T}{K} \tag{6}$$

$$K = K_0 + PK' \tag{7}$$

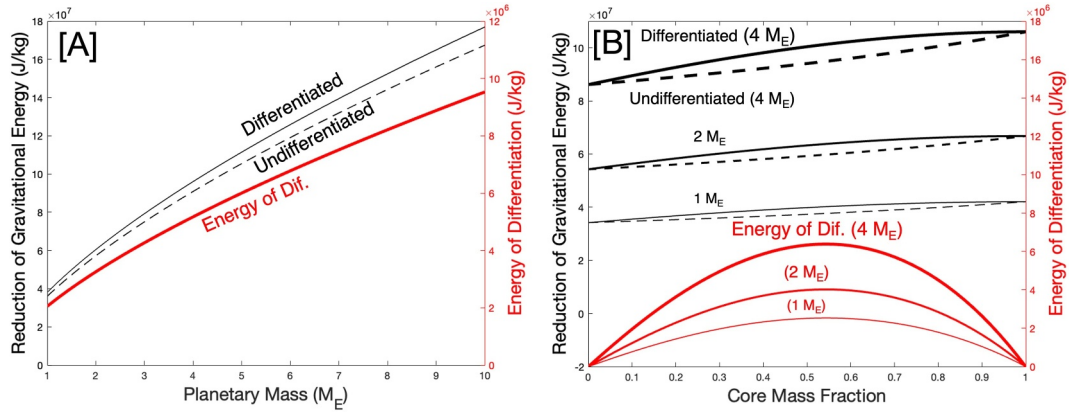

Figure 1. Energy of accretion and differentiation as a function of planetary mass and core mass fraction (CMF). (a) For planets with Earth-like CMF of 0.32 and masses between 1 and 10 Earth mass (M_E) (b) For planets with 1, 2, and 4 Earth masses and CMF from 0 to 1. The mass-normalized reductions of gravitational energy with respect to dispersed ingredients in the differentiated and undifferentiated planets are shown as black solid and dashed curves, respectively. The energies of differentiation are shown as red solid curves.

where γ is the Grüneisen parameter, T and K are the temperature and bulk modulus at pressure P, K_0 is the bulk modulus at the base pressure, and K' is the pressure derivative of the bulk modulus (Poirier, 2000).

2.4. Determine Extent of Melting in the Core

The physical state of the initial core was determined by comparing the estimated temperature profile of the core with the melting curve of iron at relevant pressures. The melting point of compressed iron was calculated based on the semi-empirical Simon-Glatzel law with parameters **a** (134.69 GPa) and **b** (0.93) based on experimental data up to 290 GPa Sinmyo et al. (2019).

$$T^m = T^*\left(\frac{P - P^*}{a} + 1\right)^b \tag{8}$$

where T* is the reference temperature of 1,811 K at a reference pressure P* at 1 bar or 0.0001 GPa.

3. Results

The target precision of our model results depend on our chosen convergence criterion of 10 kg m^{-3} in density and they are guided by the uncertainties of current exoplanet observations. Among confirmed terrestrial super-Earth exoplanets, only 8% and 6% have volume and mass uncertainties below 5%, respectively (Abushattal et al., 2022).

3.1. Energy of Differentiation

The total gravitational energy of the iron metal and silicate is reduced as the material accretes to form a planet, and it is further reduced when the metal segregates from silicate to form a layer structure (Figure S2 in Supporting Information S1). The energy of accretion corresponds to the reduction in the gravitational energy from dispersed building blocks to the undifferentiated state. The energy of differentiation corresponds to the addition reduction in gravitation energy from the undifferentiated state to the differentiated state. Our calculations of rocky planets with 1–10 Earth masses at a fixed Earth-like core mass fraction (CMF) of 0.32 show that the mass-normalized reduction of gravitational energy with respect to dispersed ingredients in both the undifferentiated and differentiated states, as well as the energy of differentiation, increases with the planet's total mass as a power law $M^{2/3}$ (Figure 1a).

For planets with variable CMFs at a fixed planet mass, we expect that the energy of differentiation approximates a bell curve anchored at zero for both fully-silicate and fully-iron planets. Indeed, our calculations for 1, 2, and 4 Earth masses show that at a given planet mass, the energy of differentiation reaches the maximum value at 55%

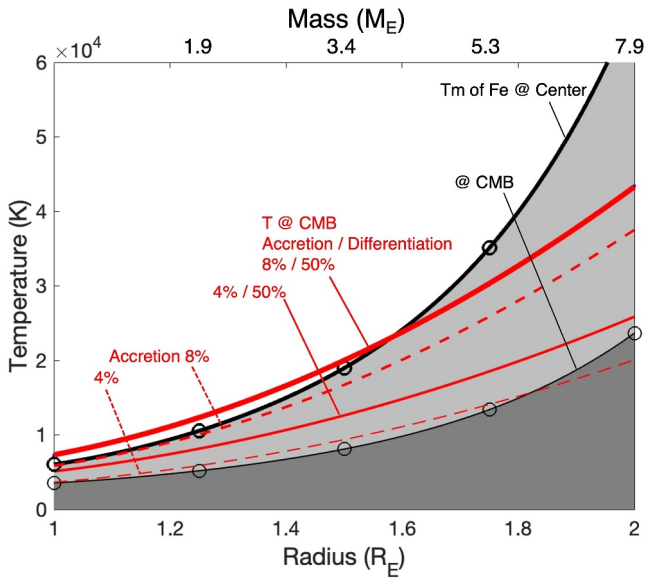

Figure 2. Extent of core melting for super-Earth planets with 1 and 2 Earth radii at a fixed CMF of 0.32. The CMB temperature in the undifferentiated state (energy of accretion only) for $f_a = 0.04$ (thin dashed red curves) or $f_a = 0.08$ (thick dashed red curves) increases with the planet radius. The CMB temperature in the differentiated state for $f_a = 0.04$ and $f_d = 0.50$ (thin solid red curve) and $f_a = 0.08$ and $f_d = 0.50$ (thick solid red curve) increases with planet radius more steeply. The melting point of iron at the CMB pressure (thin black curve) or center pressure (solid black curve) also increases with the planet radius. The dark gray, light gray, and white regions correspond to fully solid, partially molten, and full liquid states of iron in super-Earth cores.

CMF. A peak CMF occurs because the reduction of gravitational energy in the undifferentiated and differentiated states increases with the CMF following different curvatures. This peak CMF is independent of the total mass (Figure 1b).

3.2. Effect of Planetary Radius on Core Melting

From the energy of accretion and differentiation, we calculated the initial temperature at CMB of super-Earth planets for a range of heat retention factors (Figure 2). For an Earth-sized planet with a CMF of 0.32, the mass-normalized energy of accretion is $3.5{\cdot}10^7$ J·kg^{-1}, the mass-normalized energy of differentiation is $2{\cdot}10^6$ J·kg^{-1}, and the weighted average specific heat capacity of Fe and $MgSiO_3$ is 993 J·kg^{-1}·K^{-1}. Converting 4% of the energy of accretion to heat increases the internal average internal temperature by $\Delta T_G \sim 1{,}500$ K. In comparison, a complete conversion of the energy of differentiation leads to the maximum rise in temperature, $\Delta T_D \sim 2{,}000$ K.

At a fixed CMF of 0.32, the CMB temperature of Earth-sized planet increases with the planet radius. When the energy of differentiation is ignored, the CMB temperature rises as power law T (K) $= 2{,}613(R_E)^{2.87} + 1{,}000$ for $f_a = 0.04$ and $f_d = 0$, and T (K) $= 4{,}781(R_E)^{2.94} + 990$ for $f_a = 0.08$ and $f_d = 0$. When 50% of the energy of differentiation is included, the CMB temperature rises as power law T (K) $= 3813(R_E)^{2.69} + 1{,}260$ for $f_a = 0.04$ and $f_d = 0.50$, and T (K) $= 5{,}957(R_E)^{2.82} + 1{,}295$ for $f_a = 0.08$ and $f_d = 0.50$. Overall, the rise in CMB temperature due to heating by the energy of accretion or differentiation scales approximately linearly with planet volume.

To assess the extent of melting in the core, we need to compare the core temperature profile with the melting curve of iron at relevant pressures. Our structure models show that the pressures in the cores of super-Earth planets generally fall in the range of 100–1,000 GPa. We calculated the adiabatic temperature gradients of convecting cores for a range of Grüneisen parameters γ between 0.9 and 1.7 (Smith et al., 2018) and at representative base CMB temperatures of 3,600 and 8,000 K (Figure S3 in Supporting Information S1). The temperature rises at a rate of 2–5 K/GPa along the adiabats and is relatively insensitive to γ and the CMB temperature. Because the melting point of iron rises more steeply with pressure than the adiabatic temperature gradient, we can compare the temperature and the melting point of iron at the CMB to determine the extent of core melting: If the CMB temperature exceeds the melting point of iron at the CMB pressure, then the core is at least partially molten; If the CMB temperature exceeds the melting point of iron at the center, the core must be fully molten.

The structure models yielded the pressure profiles of super-Earth planets, which allowed us to calculate the melting points of iron at the core-mantle boundary (CMB) and the center (Figure 2). At a fixed CMF of 0.32, the melting temperature of iron at the CMB increases with planet radius as power law fit T (K) $= 641(R_E)^{5.00} + 3{,}070$ and that at the center increases more steeply with planet radius at power law T (K) $= 1{,}521(R_E)^{5.37} + 5{,}046$. Overall, the melting point of iron at CMB pressure roughly scales with the square of the planet volume.

Comparing the initial temperatures with the melting points of iron at the CMB of super-Earth planets with a CMF of 0.32, we found that 4% of accretional energy is insufficient to melt cores of more massive planets, whereas 8% of accretional energy would produce at least partially molten cores in all cases (Figure 2). Additional incorporation of the energy of differentiation leads to more extensive core melting. We consider retention factors on the order of 50%–100% for the energy of differentiation as most of the differentiation process occurs internally, rather than near the surface. Retaining 4% of the accretional energy and half of the differentiation energy would supply enough heat to create partially molten cores for all super-Earth planets. With 8% of the accretional energy and half of the differentiation energy, smaller super-Earths up to about four Earth masses could even develop fully molten cores.

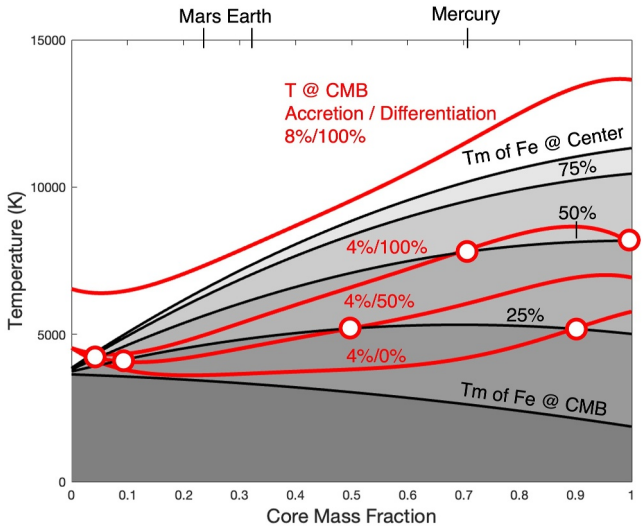

Figure 3. Extent of core melting for super-Earth planets with variable composition at a fixed one Earth radius. The red curves represent the CMB temperature as a function of CMF for various heat retention factors. The black curves represent the melting points of iron at various depths inside the core, from the CMB, 25%,50%,75% core radius below the CMB, to the center. The gray shaded regions correspond to fully solid, partially molten and full liquid states of iron in super-Earth cores.

3.3. Effect of Composition on Core Melting

For planets with variable CMF at a fixed radius of 1 R_E, the initial temperatures at CMB of super-Earth planets are calculated for a range of heat retention factors (Figure 3). The calculated initial temperatures at the CMB pressure display non-linear and complex dependence on the CMF. At 4% retention of accretion energy, the weighted average specific heat capacity of Fe and $MgSiO_3$ varies from 1,250 $J{\cdot}kg^{-1}{\cdot}K^{-1}$ for pure $MgSiO_3$ planet (CMF = 0) to 446 $J{\cdot}kg^{-1}{\cdot}K^{-1}$ for pure iron planet (CMF = 1). Accordingly, the initial CMB temperature of a nearly pure $MgSiO_3$ planet is ~5,000 K and independent of the CMF because no differentiation is involved. As the iron content increases, the CMB temperature first decreases then increases with the CMF, and it may become flat or increase again depending on the retention efficiency of the energy of differentiation. The complex dependence is due to interplay among several factors, including a positive correlation between the energy of accretion and the CMF, the bell-curve-shaped dependence of the energy of differentiation on the CMF, and a negative correlation between the average specific heat capacity and the CMF. With a higher retention of the accretional energy of 8%, the initial core temperature at CMB is higher by 2,000–4,000 K.

The melting temperature at CMB pressure decreases with CMF, because the CMB moves from the center of a nearly pure $MgSiO_3$ planet to the surface of the pure iron planet. The melting temperature at the center of the planet increases with CMF because the center pressure increases with the total mass of the planet from 150 GPa in a nearly pure $MgSiO_3$ planet to more than 1 TPa in a pure Fe planet.

For Earth-sized planets with variable CMFs, our results show that accretional energy alone at 4% retention efficiency ($f_a = 0.04$ and $f_d = 0$) would supple enough heat for planets of all compositions to be molten at least in the shallow part of the cores (Figure 3). As expected, at a given CMF, heat contribution from the energy of differentiation leads to more extensive melting in the core. For instance, for planets with CMF = 0.32% and 4% retention of accretional heat, the core is less than 10% molten at $f_d = 0$ and more than 25% molten at $f_d = 1$. Increasing the heat contribution from the energy of accretion also has a considerable influence on the extent of core melting. As an example, for planets with CMF = 0.32 and full retention of the differentiation energy, the core is less than half molten at $f_a = 0.04$ and fully molten at $f_a = 0.08$. Interpolating between these curves, we calculate that $f_a > 0.07$ is required for a fully molten core. At all scenarios of heat retention efficiencies, the extent of core melting tends to increase with the CMF. Overall, our results suggest that at $f_a = 0.04$–0.08 and $f_d = 0.50$–1.00, rocky planets universally have at least partially molten cores.

4. Discussion

4.1. Model Uncertainties

The algorithm was tested on a model Earth with a radius of 6,373 km and a core mass fraction (CMF) 32%. Our structure model of a differentiated planet with one Earth mass and an Earth-like CMF of 0.32 reproduced the Preliminary Reference Earth Model (PREM, Dziewonski & Anderson, 1981) within 1% for the density profile in the mantle and inner core, and within 3% for the gravitational acceleration and pressure profiles (Figure S4 in Supporting Information S1). The model produced excess density at the outer-core pressures, due to omitting light elements in Earth's core. The excess density near the surface is due to the use of perovskite-structured $MgSiO_3$ in the model where less dense phases are present in Earth. Our model assumed a fully molten core and added the volume of fusion to the EoS of solid iron. Applying EoS of liquid iron (Anderson & Ahrens, 1994, Table S1 in Supporting Information S1) yields a pressure profile that is within 1%. Considering that the cores of super-Earth planets may be solid or partially molten, the model uncertainties are estimated at 1%. The reasonable match with PREM despite the simplifying approximation of an $MgSiO_3$-only mantle, Fe-only core, and no phase transitions suggests that the models can provide first-order prediction of the initial thermal state of super-Earth exoplanets.

We compiled the reported EoS parameters of Fe and $MgSiO_3$ (Table S1 in Supporting Information S1) and compared the compression curves up to 1.2 TPa (Figure S5 in Supporting Information S1). The latest EoS of Fe (Smith et al., 2018) and $MgSiO_3$ (Fei et al., 2021) appear to fall near the average positions. The more massive planets with larger CMF were found to have core pressures greater than 10 TPa, where the Vinet EoS is known to display incorrect asymptotic behavior and Thomas-Fermi-Dirac becomes relevant (Seager et al., 2007 and references therein). This effect requires further study.

The effects of thermal expansion on the densities of Fe and $MgSiO_3$ have been well-documented. Fei et al. (2021) showed that, at the 0–1,000 GPa pressure range usually experienced in super-Earth interiors, increasing the temperature of $MgSiO_3$ from 300 to 7,800 K results in a decrease in density of only 3%. Similar results are seen in Morard et al. (2013), where increasing the temperature of Fe from 300 to 4000 K results in a density decrease of 4.5%. The constancy of this temperature-density relationship, regardless of pressure, suggests that the simplifying treatment of thermal effects in our models should not affect our first-order conclusions.

The Dulong-Petit law predicts a specific heat capacity of 25 $J{\cdot}mol^{-1}{\cdot}K^{-1}$ or 446 $J{\cdot}kg^{-1}{\cdot}K^{-1}$ for iron, which is about 20% less than the reported value of 29.4 $J{\cdot}mol^{-1}{\cdot}K^{-1}$ (Saxena & Eriksson, 2015). The predicted specific heat capacity of $MgSiO_3$ 125 $J{\cdot}mol^{-1}{\cdot}K^{-1}$ or 1,250 $J{\cdot}kg^{-1}{\cdot}K^{-1}$ is 10%–40% lower than the reported value of $MgSiO_3$ ilmenite at 77–111 $J{\cdot}mol^{-1}{\cdot}K^{-1}$ (Ashida et al., 1988). Because the estimated initial temperatures are generally above the Debye temperatures (Poirier, 2000), we consider the Dulong-Petit values reasonable until better constraints become available. We calculated the temperature rise based on the weighted average specific heat capacity of Fe and $MgSiO_3$ and assumed uniform temperature rise throughout the planet. In actual planets, heat loss depends on depth and convective rigor. Once the core is formed in the center of a planet and insulated by the mantle, it may be preferentially heated. These aspects need to be further studied.

The melting point of iron determined by Sinmyo et al. (2019) is up to ∼1,000 K lower than that of Anzellini et al. (2013), where the measurements reached about 200 GPa. A recent theoretical work by Cuong et at. (2022) predicted the melting curve of iron up to 4,000 GPa. At pressures below ∼400 GPa, our melting points are lower than the theoretical values. At higher pressures, however, our extrapolated melting points become higher than Cuong et al. (2022), by as much as 3,000 K at 1 TPa. Our model predictions must be updated when robust constraints on the melting curve of iron at relevant pressures become available.

4.2. Constraints on Heat Retention Efficiency

The heat retention factors in our formulation encompass a range of effects including partial conversion of gravitational energy to elastic energy stored on the planet (Birch, 1965; Flasar & Birch, 1973), heat loss through conduction, convection and evaporation, and the heat partitioning between metal-silicate, which depends on the physical mechanisms of core segregation and viscosity contrast between Fe and $MgSiO_3$ melt (Monteux et al., 2009; Rubie et al., 2015). For instance, we assumed random iron distribution within each protoplanetary body. Initial introduction of iron by impacts may lead to a heterogeneous metal distribution, which could affect the energy produced by differentiation as well as the thermal profile of the differentiated planet. Moreover, heat partitioning between metal and silicate likely differs between small metal drops settling out of molten silicate and large diapirs of core melt migrating through the solid mantle (Rubie et al., 2015). We only considered the short-term bulk heating of a rocky planet directly after accretion and differentiation, with no accounting for effects such as radiogenic heating and convective mantle cooling, which may dominate in the long run (Boujibar et al., 2020). Our energy calculations also disregard any effects of planetary impacts, which can have significant implications for planetary thermodynamics, but are far too planet-specific to be incorporated into a general-purpose model.

The heat retention efficiencies directly influence the extent of core melting in Earth-sized rocky planets (Figure 4). Boujibar et al. (2020) considered the heat contribution from the energy of accretion and adopted a retention factor of 4%. For an Earth-like CMF of 30%, this does not provide enough heat to melt the entire core of the nascent Earth. An additional contribution of differentiation energy would generate a partially molten core, but even full retention of differentiation energy does not supply enough heat to produce a fully molten core in early Earth (Figure 3). Given that the initial core was probably fully molten (Buffett et al., 1996), our results suggest that a minimum retention efficiency of accretion energy at 7% at full retention of the energy of differentiation ($f_a = 0.07, f_d = 1.00$).

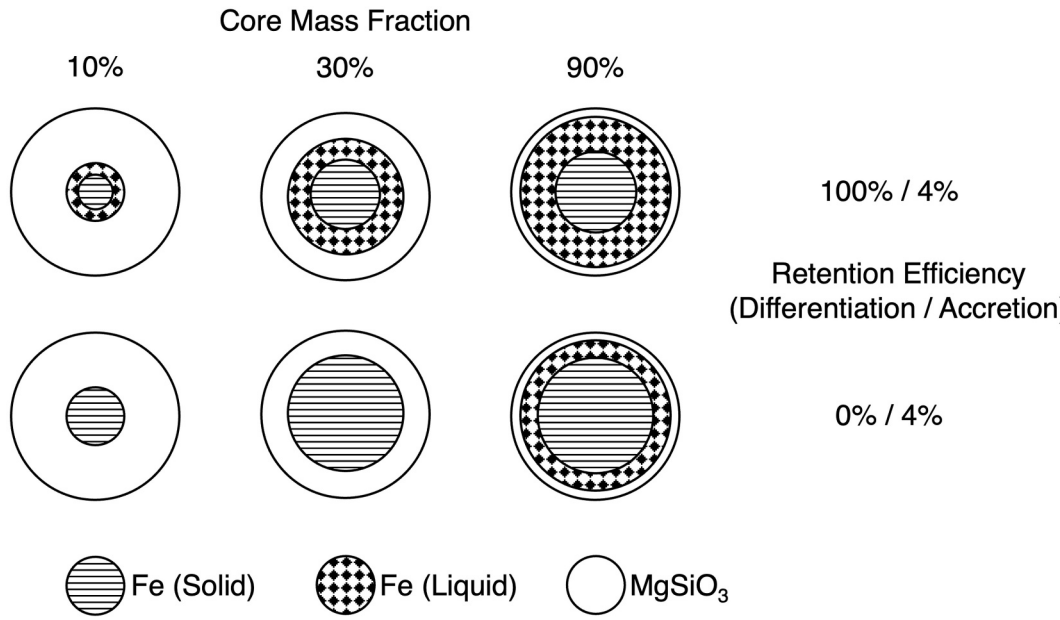

Figure 4. Cartoon illustrations of core melting in Earth-sized planets with variable core mass fractions (CMFs) for selected scenarios of heat retention factors. As the retention efficiency of differentiation energy increases from 0% (lower row) to 100% (upper low) at a fixed retention efficiency of accretion energy (4%), partially molten cores become common at a wide range of CMFs. At a given set of heat retention factors, the extent of core melting increases as CMF increases from 10% through 30% (Earth-like) to 90%. Data are found in Figure 3.

The minimum retention efficiency of accretional energy could be lower if we consider the presence of the light elements in the core, which generally reduces the melting point of core alloys (e.g., Li, 2021). This value is also subject to modification if other heat sources, such as radiogenic heating, are considered. Most sources of radiogenic heat exist outside the core and have little contribution to core melting (Ruedas, 2017). However, the contribution of radiogenic heating shows a complex dependence on the bulk composition of various radioactive isotopes and planetary age. Moreover, the cumulative radiogenic heat has been shown to increase over time as a percentage of a planet's internal heat budget, making up a significant percentage of the internal heat of modern-day Earth (Jaupart et al., 2015). These factors require further research.

4.3. Implications for Early Dynamo

Our results can be applied to assess the likelihood of dynamo development in young super-Earth exoplanets discovered by recent and future studies. At a fixed CMF, larger planets are more likely to have a molten core (Figure 2), and therefore to satisfy one of the requirements to generate a dynamo. For Earth-sized planets, our results suggest a subset of planets of interest for future study, those near 55% CMF, based on their theoretically higher initial heat and increased potential for dynamo development. Previous work surveying a sample of 207 Earth-sized exoplanets and 680 super-Earth exoplanets showed a significant population of terrestrial planets near this maximum (Howe et al., 2014).

Scaling laws have been developed for predicting magnetic field strength from the internal heat budget, and they work well for high-flux objects such as low-mass stars (Christensen, 2010). For super-Earth exoplanets, fuller pictures of dynamo development will require the incorporation of additional factors, including secular cooling, radiogenic heating, compositional variation in both core and mantle, and inner core growth (e.g., Buffett, 2000; O'Rourke & Stevenson, 2016) transitions. Nevertheless, using the available outer-core heat budget as a proxy for heat flux, we made crude estimates on the relative intensities of magnetic fields of super-Earth exoplanets (Figure S6 in Supporting Information S1). At a fixed Earth-like composition, the magnetic field strength is found to increase linearly with the planet radius from 0.30 mT at 1 R_E to 0.65 mT at 2 R_E. For planets with one Earth radius, the magnetic field strength reaches a maximum of 0.32 mT at about 60% core mass fraction. This peak is slightly

higher than the 55% peak of energy of differentiation because the heat flux across the core-mantle boundary depends on not only the mass-normalized energy of differentiation but also on the surface area of the core that increases with the CMF. These field strengths are at the core-mantle boundary. The field intensity at the surface of the planet is generally smaller due to the magnetic flux passing through a larger area and it would be influenced by the overlying mantle (Aubert et al., 2009; Driscoll & Olson, 2011). While an estimate of the surface field would more directly inform the detectability of the field, it is beyond the scope of this work.

4.4. Application to Known Planets

While this study considered mainly Earth-like parameters as a convenient baseline to determine various temperature relationships, the underlying principles can be applied to exoplanets. With planetary radius and core mass fraction data as inputs, we can assess the thermal state of the planet at the time of its formation and explore the implications for the development of magnetic fields and habitability (Wagner et al., 2012). For example, 55 Cancri E is a super-Earth exoplanet with 8.70 M_E and 1.88 R_E, roughly a CMF of 11%. Recent thermodynamic interrogation of the modern-day thermal state of its interior suggests that the radiative surface temperature of 55 Cancri energy falls between 2,000 and 3,500 K (Meier et al., 2023). We estimated that core-mantle differentiation of this planet produced ~8.7 10^6 J kg^{-1} of energy. Thus, we predict that this planet, directly after differentiation, would have an average internal temperature of more than 12,000 K if conservative heat retention efficiencies of $f_a = 0.04$ and $f_d = 0.50$ are assumed. With a CMB pressure of 1900 GPa, this would suggest that its initial core is likely partially molten.

By considering the energy of differentiation, our model of Earth predicts a higher initial core temperature than Boujibar et al. (2020). Geodynamo models have shown that, in the first 0.5 to 1.0 billion years of the Earth's history, thermal buoyancy may have provided the main driving force for rapid convection of a fully molten core (Buffett, 2000; Landeau et al., 2022; Nimmo, 2015; Olson, 2013). As the core cooled and solidification began, thermo-chemical buoyancy force associated with the growth of the inner core supplied as much as 80% of the dynamo power (Buffett, 2000). However, the inner core may have existed only in the recent 0.5 to 1.0 billion years, which implies a conflict between the long-lasting geomagnetic field and the high thermal conductivity of the core (Biggin et al., 2015; Labrosse, 2015; Olson, 2013). The proposed solutions to this "new core paradox" include thermo-chemical convection, precession, and tides. Of these, convection, aided by exsolution of magnesium oxide or silicon dioxide (e.g., Badro et al., 2016; Hirose et al., 2017; Du et al., 2017; O'Rourke & Stevenson, 2016), appears the most likely to be responsible for powering the dynamo before the inner core is formed. Several key parameters, including the evolution of available heat, remain unknown (Landeau et al., 2022).

Our results can help resolve the new core paradox, particularly in relation to the hot core solution (Driscoll & Davies, 2023). This solution, previously described as unlikely, allows for the generation of a geodynamo in the Earth's core prior to inner core formation given an initial core temperature greater than 6,000 K. Such temperatures are easily achievable at 1 R_E given $f_a = 0.08$, and are even accessible at $f_a = 0.04$ for planets larger than 1.1 R_E. These results indicate that the hot core solution may be more viable than previously thought. While the scope of this work focuses on super-Earth planets, the method can also be applied to sub-Earth rocky planets. Mars, for example, can be calculated to have an initial CMB temperature of near 1,800 K, assuming $f_a = 0.04$ and $f_d = 0.5$.

The James Webb Space Telescope has identified new exoplanets such as LHS 475-b and provided insights into the thermal environments of known exoplanets such as TRAPPIST-1 (Lustig-Yaeger et al., 2019, 2023). As new developments in planetary measurements arrive, predictions of the presence and strength of dynamos will become more accurate. Determining the structure of exoplanets, including gaseous envelopes and the presence of volatiles, is an important consideration, as our findings apply most directly to super-Earth planets of $MgSiO_3$ and Fe composition. While our methods can approximate the initial thermal states of exoplanets, there is further work to be done in bridging the gap between the initial and current states. Thermodynamic simulations, such as that performed by Meier et al. (2023), should provide a more systematic picture of how the thermal states of exoplanets evolve.

5. Conclusions

We calculated the energies generated during the accretion and differentiation of model super-Earth planets consisting of iron (Fe) and silicate ($MgSiO_3$) across a variety of parameters including mass and composition. For planets with an Earth-like iron to silicate ratio, the energy of accretion and the energy of differentiation increase

with planet mass as a power law, roughly $M^{2/3}$. For planets with one Earth radius, the energy of accretion increases with the core mass fraction (CMF), whereas the energy of differentiation peaks at about 0.55 CMF.

With specific heat capacities calculated using the Dulong-Petit law, we predicted the initial thermal states of super-Earth planets. Although the energy of accretion is one order of magnitude higher than the energy of differentiation, a larger fraction of differentiation energy may be retained because the core segregation mainly takes place inside a planet, and therefore differentiation may contribute a significant amount of heat to a nascent planet. In a planet with one Earth radius and ∼30% core mass fraction, for example, 4% of accretional energy and 50% of differentiation energy contribute equally to the total temperature rise associated with accretion and differentiation.

We applied Rose-Vinet equations of state to model the pressure and temperature profiles in these super-Earth planets. Despite several simplifying assumptions, our model planet with 1 R_E and 0.32 CMF reproduced the pressure profile of PREM within 1%, thus demonstrating the validity of the method in providing first-order insights into the initial thermal states of super-Earth planets.

For planets with an Earth-like CMF of 0.32, we found that the initial temperature at the core-mantle boundary (CMB) rises as R^3, almost linearly with planet volume. In comparison, the melting point of iron at the CMB pressure rises more steeply, as R^5 or roughly V^2. We predict partial melting of core after differentiation in all but the largest planets up to 2 R_E, even with 4% retention of accretion energy and not accounting for the energy of differentiation. Planets with up to four Earth mass are expected to have fully molten cores if 8% of the accretion energy and half of the differentiation energy contribute to heating.

Our study revealed more complex behavior in planets of Earth radius and variable compositions, due to the combined effects of CMF on the energies of accretion and differentiations as well as the specific heat capacity. We predict that at least partially molten cores are common in Earth-sized rocky planets for a wide range of heat retention efficiencies, from 4% to 8% for the energy of accretion and from 50% to 100% for the energy of differentiation. At the high ends of these ranges (8% accretion and 100% differentiation), entirely molten cores are expected for all compositions from pure silicate to pure iron.

Complementary to existing work on energy of accretion (Boujibar et al., 2020), we showed that incorporating the thermal effects of differentiation within rocky planets leads to much more extensive melting in their initial cores, thus enhancing the potential for running early dynamos and increasing the intensity of young magnetic fields. The addition of the energy of accretion also brought Boujibar et al. (2020)'s results more in line with the largely molten core in the present-day Earth. If we ignore other heat sources such as impacts and radiogenic heating are, and the effects of light elements on the melting point of core-alloys, then at least ∼7% of the accretion energy must be retained to produce a fully molten core in Earth after its formation.

The planetary models in this study can be manipulated in a variety of ways to inform the relationships between planetary structure and thermal evolution. While a full characterization of the structure-temperature relationships requires more insight into specific planetary history, formation conditions, and volatile element compositions, understanding the general influences of planet mass and composition of various categories of provides a first order understanding of their thermal states, with broad implications for the potential of super-Earths to support life.

Conflict of Interest

The authors declare no conflicts of interest relevant to this study.

Acknowledgments
We thank Alex Dewey and Charles Weber for their contributions to early versions of this work. We thank Professor David Stevenson (Caltech), Professor Francis Nimmo (UCSC), and Professor Tushar Mittal (PSU) for sharing important insights about calculating the energy of accretion and differentiation. The manuscript benefited from two highly constructive and thorough reviews. This research was partially supported by NSF AST 1344133 and NSF EAR2317024.

Data Availability Statement

The codebase and data sets used in this research have been frozen and stored on zenodo. They are made available in the citation reference White and Li (2024).

References

Abushattal, A. A., Kraishan, A. F., & Alshamaseen, O. S. (2022). The exoplanets catalogues and archives: An astrostatistical analysis. In *Communications of the Byurakan astrophysical observatory* (pp. 235–241). National Academy of Sciences of the Republic of Armenia. https://doi.org/10.52526/25792776-22.69.2-235

Anderson, W. W., & Ahrens, T. J. (1994). An equation of state for liquid iron and implications for the Earth's core. *Journal of Geophysical Research*, *99*(B3), 4273–4284. https://doi.org/10.1029/93JB03158

Anzellini, S., Dewaele, A., Mezouar, M., Loubeyre, P., & Morard, G. (2013). Melting of iron at Earth's inner core boundary based on fast X-ray diffraction. *Science*, *340*(6131), 464–466. https://doi.org/10.1126/science.1233514

Ashida, T., Kume, S., Ito, E., & Navrotsky, A. (1988). $MgSiO_3$ ilmenite: Heat capacity, thermal expansivity, and enthalpy of transformation. *Physics and Chemistry of Minerals*, *16*(3), 239–245. https://doi.org/10.1007/BF00220691

Aubert, J., Labrosse, S., & Poitou, C. (2009). Modelling the palaeo-evolution of the geodynamo. *Geophysical Journal International*, *179*(3), 1414–1428. https://doi.org/10.1111/j.1365-246x.2009.04361.x

Badro, J., Siebert, J., & Nimmo, F. (2016). An early geodynamo driven by exsolution of mantle components from Earth's core. *Nature*, *536*(7616), 326–328. https://doi.org/10.1038/nature18594

Biggin, A. J., Piispa, E. J., Pesonen, L. J., Holme, R., Paterson, G. A., Veikkolainen, T., & Tauxe, L. (2015). Palaeomagnetic field intensity variations suggest Mesoproterozoic inner-core nucleation. *Nature*, *526*(7572), 245–248. https://doi.org/10.1038/nature15523

Birch, F. (1965). Energetics of core formation. *Journal of Geophysical Research*, *70*(24), 6217–6221. https://doi.org/10.1029/JZ070i024p06217

Boujibar, A., Driscoll, P., & Fei, Y. (2020). Super-Earth internal structures and initial thermal states. *Journal of Geophysical Research: Planets*, *125*(5). https://doi.org/10.1029/2019je006124

Buffett, B. A. (2000). Earth's core and the geodynamo. *Science*, *288*(5473), 2007–2012. https://doi.org/10.1126/science.288.5473.2007

Buffett, B. A., Huppert, H. E., Lister, J. R., & Woods, A. W. (1996). On the thermal evolution of the Earth's core. *Journal of Geophysical Research*, *101*(B4), 7989–8006. https://doi.org/10.1029/95JB03539

Cambioni, S., Jacobson, S. A., Emsenhuber, A., Asphaug, E., Rubie, D. C., Gabriel, T. S. J., et al. (2021). The effect of inefficient accretion on planetary differentiation. *The Planetary Science Journal*, *2*(3), 93. American Astronomical Society. https://doi.org/10.3847/psj/abf0ad

Christensen, U. R. (2010). Dynamo scaling laws and applications to the planets. *Space Science Reviews*, *152*(1–4), 565–590. https://doi.org/10.1007/s11214-009-9553-2

Cuong, T. D., Hoc, N. Q., Trung, N. D., Thao, N. T., & Phan, A. D. (2022). Theoretical predictions of melting behaviors of HCP iron up to 4000 GPa. *Physical Review B*, *106*(9), 94103. https://doi.org/10.1103/PhysRevB.106.094103

Driscoll, P., & Davies, C. (2023). The "new core paradox": Challenges and potential solutions. *Journal of Geophysical Research: Solid Earth*, *128*(1), e2022JB025355. https://doi.org/10.1029/2022jb025355

Driscoll, P., & Olson, P. (2011). Optimal dynamos in the cores of terrestrial exoplanets: Magnetic field generation and detectability. *Icarus*, *213*(1), 12–23. https://doi.org/10.1016/j.icarus.2011.02.010

Du, Z., Jackson, C., Bennett, N., Driscoll, P., Deng, J., Lee, K. K. M., et al. (2017). Insufficient energy from MgO exsolution to power early geodynamo. *Geophysical Research Letters*, *44*(22), 11376. https://doi.org/10.1002/2017gl075283

Duffy, T., Madhusudhan, N., & Lee, K. K. M. (2015). Mineralogy of super-Earth planets. *Treatise on Geophysics*, 149–178. Elsevier. https://doi.org/10.1016/b978-0-444-53802-4.00053-1

Dziewonski, A. M., & Anderson, D. L. (1981). Preliminary reference Earth model. *Physics of the Earth and Planetary Interiors*, *25*(4), 297–356. Elsevier BV. https://doi.org/10.1016/0031-9201(81)90046-7

Fei, Y., Seagle, C. T., Townsend, J. P., McCoy, C. A., Boujibar, A., Driscoll, P., et al. (2021). Melting and density of $MgSiO_3$ determined by shock compression of bridgmanite to 1254GPa. *Nature Communications*, *12*(1), 876. Springer Science and Business Media LLC. https://doi.org/10.1038/s41467-021-21170-y

Flasar, F. M., & Birch, F. (1973). Energetics of core formation: A correction. *Journal of Geophysical Research*, *78*(26), 6101–6103. https://doi.org/10.1029/JB078i026p06101

Gunell, H., Maggiolo, R., Nilsson, H., Wieser, G. S., Slapak, R., Lindkvist, J., et al. (2018). Why an intrinsic magnetic field does not protect a planet against atmospheric escape. *Astronomy and Astrophysics*, *614*, L3. https://doi.org/10.1051/0004-6361/201832934

Hirose, K., Morard, G., Sinmyo, R., Umemoto, K., Hernlund, J., Helffrich, G., & Labrosse, S. (2017). Crystallization of silicon dioxide and compositional evolution of the Earth's core. *Nature*, *543*(7643), 99–102. https://doi.org/10.1038/nature21367

Howe, A. R., Burrows, A., & Verne, W. (2014). Mass-radius relations and core-envelope decompositions of super-earths and sub-neptunes. *The Astrophysical Journal*, *787*(2), 173. American Astronomical Society. https://doi.org/10.1088/0004-637x/787/2/173

Hu, R., Beichman, C. A., Brain, D., Chen, P., Damiano, M., Dawson, R., et al. (2019). The super-Earth opportunity—Search for habitable exoplanets in the 2020s (Version 1). arXiv. https://doi.org/10.48550/ARXIV.1903.05258

Izidoro, A., Schlichting, H. E., Isella, A., Dasgupta, R., Zimmermann, C., & Bitsch, B. (2022). The exoplanet radius valley from gas-driven planet migration and breaking of resonant chains. *The Astrophysical Journal Letters*, *939*(2), L19. American Astronomical Society. https://doi.org/10.3847/2041-8213/ac990d

Jaupart, C., Labrosse, S., Lucazeau, F., & Mareschal, J. C. (2015). 7.06—Temperatures, heat, and energy in the mantle of the Earth. In G. Schubert (Ed.), *Treatise on Geophysics* (2nd ed., pp. 223–270). Elsevier.

Kaltenegger, L. (2017). How to characterize habitable worlds and signs of life. *Annual Review of Astronomy and Astrophysics*, *55*(1), 433–485. Annual Reviews. https://doi.org/10.1146/annurev-astro-082214-122238

Komabayashi, T., & Fei, Y. (2010). Internally consistent thermodynamic database for iron to the Earth's core conditions. *Journal of Geophysical Research*, *115*(B3). https://doi.org/10.1029/2009jb006442

Labrosse, S. (2015). Thermal evolution of the core with a high thermal conductivity. *Physics of the Earth and Planetary Interiors*, *247*, 36–55. https://doi.org/10.1016/j.pepi.2015.02.002

Landeau, M., Fournier, A., Nataf, H.-C., Cébron, D., & Schaeffer, N. (2022). Sustaining Earth's magnetic dynamo. *Nature Reviews Earth & Environment*, *3*(4), 1–15. https://doi.org/10.1038/s43017-022-00264-1

Li, J. (2019). Chen B, Mookherjee M and Morard G, Carbon versus other light elements in the core—A combined geochemical and geophysical perspective. In B. Orcutt, I. Daniel, & R. Dasgupta (Eds.), *Earth carbon past to present* (pp. 40–65). Cambridge University Press. https://doi.org/10.1017/9781108677950

Li, J. (2021). Composition of the Earth's core. In R. Arevalo (Ed.), *Encyclopedia of geology* (2nd ed., pp. 150–163). Elsevier Ltd.

Li, J., & Fei, Y. (2014). 3.15—Experimental constraints on core composition. In H. D. Holland & K. K. Turekian (Eds.), *Treatise on geochemistry* (2nd ed., pp. 527–557). Elsevier. https://doi.org/10.1016/B978-0-08-095975-7.00214-X

Liu, J., Dorfman, S. M., Zhu, F., Li, J., Wang, Y., Zhang, D., et al. (2018). Valence and spin states of iron are invisible in Earth's lower mantle. *Nature Communications*, *9*(1), 1284. Springer Science and Business Media LLC. https://doi.org/10.1038/s41467-018-03671-5

Lustig-Yaeger, J., Fu, G., May, E. M., Ceballos, K. N. O., Moran, S. E., Peacock, S., et al. (2023). A JWST transmission spectrum of the nearby Earth-sized exoplanet LHS 475 b. *Nature Astronomy*, *7*(11), 1317–1328. Springer Science and Business Media LLC. https://doi.org/10.1038/s41550-023-02064-z

Lustig-Yaeger, J., Meadows, V. S., & Lincowski, A. P. (2019). The detectability and characterization of the TRAPPIST-1 exoplanet atmospheres with JWST. *The Astronomical Journal*, *158*(1), 27. American Astronomical Society. https://doi.org/10.3847/1538-3881/ab21e0

Meier, T. G., Bower, D. J., Lichtenberg, T., Hammond, M., & Tackley, P. J. (2023). Interior dynamics of super-Earth 55 Cancri e. *Astronomy & Astrophysics*, *678*, A29. EDP Sciences. https://doi.org/10.1051/0004-6361/202346950

Monteux, J., Jellinek, A. M., & Johnson, C. L. (2011). Why might planets and moons have early dynamos? *Earth and Planetary Science Letters*, *310*(3), 349–359. https://doi.org/10.1016/j.epsl.2011.08.014

Monteux, J., Ricard, Y., Coltice, N., Dubuffet, F., & Ulvrova, M. (2009). A model of metal–silicate separation on growing planets. *Earth and Planetary Science Letters*, *287*(3), 353–362. https://doi.org/10.1016/j.epsl.2009.08.020

Morard, G., Siebert, J., Andrault, D., Guignot, N., Garbarino, G., Guyot, F., & Antonangeli, D. (2013). The Earth's core composition from high pressure density measurements of liquid iron alloys. *Earth and Planetary Science Letters*, *373*, 169–178. Elsevier BV. https://doi.org/10.1016/j.epsl.2013.04.040

Nimmo, F. (2015). 9.08—Thermal and compositional evolution of the core. In G. Schubert (Ed.), *Treatise on geophysics* (2nd ed., pp. 201–219). Elsevier.

Olson, P. (2013). The new core paradox. *Science*, *342*(6157), 431–432. https://doi.org/10.1126/science.1243477

O'Rourke, J. G., & Stevenson, D. J. (2016). Powering Earth's dynamo with magnesium precipitation from the core. *Nature*, *529*(7586), 387–389. Springer Science and Business Media LLC. https://doi.org/10.1038/nature16495

Poirier, J.-P. (2000). *Introduction to the physics of the Earth's interior* (p. 326). Cambridge University Press.

Rubie, D. C., Jacobson, S. A., Morbidelli, A., O'Brien, D. P., Young, E. D., de Vries, J., et al. (2015). Accretion and differentiation of the terrestrial planets with implications for the compositions of early-formed Solar System bodies and accretion of water. *Icarus*, *248*, 89–108. Elsevier BV. https://doi.org/10.1016/j.icarus.2014.10.015

Ruedas, T. (2017). Radioactive heat production of six geologically important nuclides. *Geochemistry, Geophysics, Geosystems*, *18*(9), 3530–3541. American Geophysical Union (AGU). https://doi.org/10.1002/2017gc006997

Saxena, S. K., & Eriksson, G. (2015). Thermodynamics of iron at extreme pressures and temperatures. *Journal of Physics and Chemistry of Solids*, *84*, 70–74. https://doi.org/10.1016/j.jpcs.2015.03.006

Seager, S., Kuchner, M., Hier-Majumder, C. A., & Militzer, B. (2007). Mass-radius relationships for solid exoplanets. *The Astrophysical Journal*, *669*(2), 1279–1297. American Astronomical Society. https://doi.org/10.1086/521346

Sinmyo, R., Hirose, K., & Ohishi, Y. (2019). Melting curve of iron to 290 GPa determined in a resistance-heated diamond-anvil cell. *Earth and Planetary Science Letters*, *510*, 45–52. Elsevier BV. https://doi.org/10.1016/j.epsl.2019.01.006

Smith, R. F., Fratanduono, D. E., Braun, D. G., Duffy, T. S., Wicks, J. K., Celliers, P. M., et al. (2018). Equation of state of iron under core conditions of large rocky exoplanets. *Nature Astronomy*, *2*(6), 452–458. Springer Science and Business Media LLC. https://doi.org/10.1038/s41550-018-0437-9

Spiegel, D. S., Fortney, J. J., & Sotin, C. (2013). Structure of exoplanets. *Proceedings of the National Academy of Sciences of the United States of America*, *111*(35), 12622–12627. Proceedings of the National Academy of Sciences. https://doi.org/10.1073/pnas.1304206111

Wagner, F. W., Tosi, N., Sohl, F., Rauer, H., & Spohn, T. (2012). Rocky super-Earth interiors. *Astronomy & Astrophysics*, *541*, A103. EDP Sciences. https://doi.org/10.1051/0004-6361/201118441

White, N., & Li, J. (2024). Data and code for "Initial thermal states of super-Earth exoplanets and implications for early dynamos." (Version 2) [Dataset & Code]. *Zenodo*. https://doi.org/10.5281/zenodo.11459518

Zeng, L., Jacobsen, S. B., Hyung, E., Levi, A., Nava, C., Kirk, J., et al. (2021). New perspectives on the exoplanet radius gap from a mathematica tool and visualized water equation of state. *The Astrophysical Journal*, *923*(2), 247. American Astronomical Society. https://doi.org/10.3847/1538-4357/ac3137

References From the Supporting Information

Caracas, R., & Cohen, R. E. (2005). Effect of chemistry on the stability and elasticity of the perovskite and post-perovskite phases in the $MgSiO_3$-$FeSiO_3$-Al_2O_3 system and implications for the lowermost mantle. *Geophysical Research Letters*, *32*(16). American Geophysical Union (AGU). https://doi.org/10.1029/2005gl023164

Dewaele, A., & Garbarino, G. (2017). Low temperature equation of state of iron. *Applied Physics Letters*, *111*(2). AIP Publishing. https://doi.org/10.1063/1.4989688

Garai, J., Chen, J., & Telekes, G. (2011). PVT equation of state of epsilon iron and its densities at inner core conditions. *American Mineralogist*, *96*(5–6), 828–832. Mineralogical Society of America. https://doi.org/10.2138/am.2011.3612

Karki, B. B., Wentzcovitch, R. M., de Gironcoli, S., & Baroni, S. (2001). First principles thermoelasticity of $MgSiO_3$-perovskite: Consequences for the inferred properties of the lower mantle. *Geophysical Research Letters*, *28*(14), 2699–2702. https://doi.org/10.1029/2001gl012910

Lin, Y., Cohen, R. E., Stackhouse, S., Driver, K. P., Militzer, B., Shulenburger, L., & Kim, J. (2014). Equations of state and stability of $MgSiO_3$ perovskite and post-perovskite phases from quantum Monte Carlo simulations. *Physical Review B*, *90*(18), 184103. American Physical Society (APS). https://doi.org/10.1103/physrevb.90.184103

Mao, H. K., Wu, Y., Chen, L. C., Shu, J. F., & Jephcoat, A. P. (1990). Static compression of iron to 300 GPa and Fe0.8Ni0.2 alloy to 260 GPa: Implications for composition of the core. *Journal of Geophysical Research*, *95*(B13), 21737–21742. American Geophysical Union (AGU). https://doi.org/10.1029/jb095ib13p21737

Oganov, A. R., & Ono, S. (2004). Theoretical and experimental evidence for a post-perovskite phase of MgSiO3 in Earth's D″ layer. *Nature*, *430*(6998), 445–448. Springer Science and Business Media LLC. https://doi.org/10.1038/nature02701

Ono, S., Kikegawa, T., Hirao, N., & Mibe, K. (2010). High-pressure magnetic transition in hcp-Fe. *American Mineralogist*, *95*(5–6), 880–883. Mineralogical Society of America. https://doi.org/10.2138/am.2010.3430

Sakai, T., Ohtani, E., Hirao, N., & Ohishi, Y. (2011). Stability field of the hcp-structure for Fe, Fe-Ni, and Fe-Ni-Si alloys up to 3 Mbar. *Geophysical Research Letters*, *38*(9). American Geophysical Union (AGU). https://doi.org/10.1029/2011gl047178

Stixrude, L., & Cohen, R. E. (1993). Stability of orthorhombic MgSiO3 perovskite in the Earth's lower mantle. *Nature*, *364*(6438), 613–616. Springer Science and Business Media LLC. https://doi.org/10.1038/364613a0

Tsuchiya, J., Tsuchiya, T., & Wentzcovitch, R. M. (2005). Vibrational and thermodynamic properties of $MgSiO_3$ postperovskite. *Journal of Geophysical Research*, *110*(B2). American Geophysical Union (AGU). https://doi.org/10.1029/2004jb003409

Yamazaki, D., Ito, E., Yoshino, T., Yoneda, A., Guo, X., Zhang, B., et al. (2012). P-V-T equation of state for ε-iron up to 80 GPa and 1900 K using the Kawai-type high pressure apparatus equipped with sintered diamond anvils. *Geophysical Research Letters*, *39*(20). American Geophysical Union (AGU). https://doi.org/10.1029/2012gl053540